JTTEE5 12:508-522
© ASM International

Peer Reviewed

Computational Study and Experimental Comparison of the In-Flight Particle Behavior for an External Injection Plasma Spray Process

K. Remesh, S.C.M. Yu, H.W. Ng, and C.C. Berndt

(Received 24 September 2001; in revised form 23 April 2003)

A three-dimensional computational fluid dynamic (CFD) analysis using Fluent V5.4 was conducted on the in-flight particle behavior during the plasma spraying process with external injection. The spray process was modeled as a steady jet issuing from the torch nozzle via the heating of the arc gas by an electric arc within the nozzle. The stochastic discrete model was used for the particle distribution. The particle temperature, velocity, and size inside the plasma plume at a specified standoff distance have been investigated. The results show that carrier gas flow rate variation from 2 standard liters per minute (slm) to 4.0 slm can increase the centerline particle mean temperature and mean velocity by 10% and 16%, respectively, at the specified standoff distance. A further increase of the carrier gas flow rate to 6 slm did not change the particle temperature, but the particle velocity was decreased by 20%. It was also found that an increase in the total arc gas flow rate from 52 slm to 61 slm, with all other process parameters unchanged, resulted in a 17% higher particle velocity, but 6% lower particle temperature. Some of these computational findings were experimentally confirmed by Kucuk et al.[1] For a given process parameter setting, the kinetic and thermal energy extracted by the particles reached a maximum for carrier gas flow rate of about 3.5-4.0 slm.

Keywords atmospheric plasma spray, CFD modeling, in-flight diagnostics, particle behavior

1. Introduction

The microstructural characteristics of thermal spray coatings depend strongly on the velocity, temperature, and size of the particles upon impact against the substrate. Generating coatings of good quality or any improvement on spray efficiency requires a detailed understanding of the plasma jet and its interaction with the spray particles. It is therefore of vital importance to characterize the particle behavior inside the plasma plume both computationally and experimentally.

A number of numerical modeling studies[2-4] for the plasma spray process have previously been published. The study by Wan et al.[2] presented a comprehensive model for plasma spraying with consideration of heating, melting, evaporation, and resolidification of particles during their in-flight process. A more recent work by Ahmed and Bergman[3] included the effect of carrier gas flow on the particle performance and the interaction of carrier gas with arc gas. In their work, the effects of carrier gas flow on the particle deposition of uniform sized, nanostructured particles were considered. It was found that the carrier gas played a major role in determining the particle trajectory and dispersion of the sprayed particles through mixing between the two streams and the level of turbulence generated. It was further reported by Ang et al.[4,5] that varying the carrier gas flow rate would affect the particle behavior by altering the injection velocity and, hence, particle trajectory. This behavior would in turn influence the deposition characteristics.

Recently, Williamson et al.[6] presented an interesting work in which all the phenomena that may influence the particle behavior inside the plasma plume were segregated and the effects of individual parameters that would affect the particle behavior were studied. It was found from the analysis that for the typical plasma jet injection conditions considered in the analysis, particle dispersion in the injection direction is most significantly affected (in the order of decreasing importance) by: particle size distribution, injection velocity distribution, turbulence, injection direction distribution, and particle density distribution.

Simulation studies, which consider the effect of carrier gas on particle behavior with simultaneous injection of multi-sized particles, have not been reported. In the current investigation, a three-dimensional study for the plasma spray process with an Ar/H_2 plasma, N_2 carrier gas, and yttria-partially-stabilized zirconia (YSZ) as the injected particles are reported. In the current investigation, the carrier gas flow rate is chosen to be the main parameter for consideration.

In typical plasma spray process, the carrier gas flow rate (typically 5 slm) is not insignificant compared with the arc gas flow rate (typically 50 slm); therefore, it may cool the plasma jet. The transverse injection velocity of particles into the plasma may considerably alter the particle behavior. Depending on the carrier gas flow rate which determines the particle injection velocity and the momentum acquired by the particles, the particles may experience the following: penetrate into the plasma plume emerging at the opposite side, reside in the central core of the plasma plume, or rebound without entering the plume. Also, the mixing of arc gas with carrier gas would alter the transport properties of the plasma plume.

K. Remesh, S.C.M. Yu, and **H.W. Ng,** School of Mechanical & Production Engineering, Nanyang Technological University, Nanyang Avenue, Singapore 639798; and **C.C. Berndt,** Department of Materials Science and Engineering, Stony Brook University, Stony Brook, NY 11794-2275. Contact e-mail: mcmyu@ntu.edu.sg.

A common problem encountered in plasma spray research is a suitable method to compare simulated results with those obtained experimentally. The reported experimental temperature, velocity, and size measurements are the ensemble average of particle behavior parameters. On the other hand, in simulation these values are the instantaneous individual values that make comparisons to the practical measurements difficult. A new methodology was developed in this work to compare the simulated results directly with those of the experimental measurements.

The work by Wan et al.[2] pointed out the necessity of a three-dimensional model for this analysis because the plume will not be symmetrical due to the effects of the carrier gas. To achieve the above objectives, a three-dimensional computational fluid dynamics (CFD) study for plasma interaction with sprayed particles (taking into consideration process parameters such as torch power, Ar-H_2 volume fraction, carrier gas flow rate, and stand off distance) have been carried out on a Metco 3MB torch with a GH nozzle. Some comparisons of the simulation with measurements by Kucuk et al.[1] are also presented.

Nomenclature

A_p	particle surface area, m^2
c	molar concentration of species, mol/m^3
C_D	drag coefficient, dimensionless
c_p	specific heat capacity, J/kgK
D_p	particle diameter, m
D_{ij}	diffusion coefficient, m^2/s
F_D	drag force experienced by particle, N
h	heat transfer coefficient, W/m^2K
H_{sf}	latent heat of melting, J/kg
K	turbulent kinetic energy per unit mass, m^2/s^2
k	thermal conductivity, W/mK
m_p	particle mass, kg
Nu	Nusselt number, dimensionless
P	pressure, Pa
P_r	Pandtl number, dimensionless
P_{rt}	turbulent Prandtl number, dimensionless
Re	particle Reynolds number, dimensionless
t	time, s
T	gas temperature, K
T_i	turbulence intensity, %
T_{bp}	boiling point, K
T_{mp}	melting point, K
T_p	particle temperature, K
u	axial velocity, m/s
u_p	particle axial velocity, m/s
v	velocity along y-axis, m/s

Greek Symbols

α	thermal diffusivity, m^2/s
ε	dissipation rate of turbulent kinetic energy, m^2/s^3
ρ	fluid density, kg/m^3
μ	dynamic viscosity, kg/ms
ν	kinematic viscosity, m^2/s

Subscripts

amb	ambient
cg	carrier gas
l	laminar
p	particle
t	turbulent

2. Mathematical Model

The solution technique consisted of two phases. In the first phase, a steady state solution was obtained for the plasma and carrier gas flow without particle injection. In the second phase, YSZ particles were injected into the plasma gas and the calculation of their trajectories, temperature, velocities, and concentration histories were carried out.

2.1 Governing Equations

The following sections describe the mathematical equations, which govern the physical and thermo-mechanical processes within the plasma spray. Further details can be found in the Fluent User's Guide.[7]

2.1.1 Plasma Flow in 3-D Coordinates. The numerical procedures for obtaining the solution are based on the fully elliptic Navier-Stokes system of differential equations with the standard k-ε model for turbulence modeling. Here, a free turbulent DC plasma jet was considered for which the following assumptions were made:

1) The plasma stream was considered to be in chemical equilibrium.
2) The gas was represented as a chemically inert, multicomponent ideal gas with temperature dependent thermodynamic and transport properties.
3) The plasma flow was assumed to be in local thermal equilibrium (LTE), according to the work of Boulos et al.[8] This assumption allowed the assignment of a unique temperature to any region of the plasma stream.
4) The electric discharge was in steady state. The electric and magnetic forces generated by the current flow were not considered.
5) The net energy input to the arc gas was defined through the source term in the energy equation. It is assumed that the heat source is a continuum. It is well-known that the plasma arc flaps at a frequency of 1-5 kHz,[9] but this behavior may be considered as continuous with respect to the thermo-fluid events subjected upon the particles during their in-flight.
6) The flow was assumed to be straight flow only with no swirl component.

Based on the above assumptions, the conservation equations can be written in the general form as:

$$\nabla.(\rho V\phi) = \nabla.(\Gamma_\phi \nabla\phi) + S_\phi \qquad \text{(Eq 1)}$$

with ϕ as the process variable. The diffusion coefficients Γ_ϕ for the different conservation equations are given in Table 1.

The local arc phenomenon in thermal spray was not considered in this work. Instead a volume averaged source term was included in the governing energy equation to account for heating from the electric arc. The equation has the form:

Table 1 The Process Variables, Diffusion Coefficient, and Source Term for Governing Eq 1

Governing Equation	Variable, ϕ	Diffusion Coefficient, Γ_ϕ	Source Term, S_ϕ
Mass	1	…	…
Momentum	*u, v, w*	ν	…
Energy	*T*	α	P'''_{in}
Species	*c*	D_{ij}	…
Turbulence	*k*, ε	γ_t	…

$$P'''_{in} = \frac{\eta_t EI}{V} \quad \text{(Eq 2)}$$

where P'''_{in} is the volume averaged torch power input, E is the arc voltage, I is the arc current, η_t is the torch efficiency, and V is the anode volume. The power efficiency of torch was assumed to be 63% after Vardelle et al.[10]

The heat input (or rather electrical heating of the arc gas) was modeled as a heat source within the plasma torch nozzle, instead of a velocity profile at the nozzle exit as assumed by previous researchers.[2-4] Chang and Ramshaw[11] found that the assumed value of the exponent in the power law for velocity and temperature influences the plasma jet behavior, and hence the predicted particle behavior.

2.1.2 Turbulence Modeling. The effects of turbulence on mean flow were modeled using the standard k-ε model that is the most widely used turbulence model in plasma spray research. The inlet boundary conditions for the turbulence model are turbulence intensity and characteristic length. The turbulence intensity (T_i) may be defined as the ratio of the root mean square velocity fluctuation to mean flow velocity. At the arc gas inlet, (A) in Fig. 1, T_i was calculated[7]

$$T_i = 0.16(Re_{DH})^{-0.125} \quad \text{(Eq 3)}$$

where Re_{DH} is the inlet flow Reynolds number calculated on the basis of the hydraulic diameter as the characteristic length.

2.1.3 Particle Motion Formulation. The particles were modeled as discrete Lagrangian entities that exchange mass momentum and energy with the plasma. The particles were modeled by a stochastic discrete-particle model. At injection rates typical of industrial spraying conditions, the particle flow field was dilute in both concentration (less than 1000/cm^3) and volume fraction (less than 3×10^{-5}).

The particle dynamics was considered under the following assumptions:

1) Particle-to-particle interactions were neglected. This was based on the calculation that the particle-particle distance was approximately 10 times the particle diameter for the assumed uniform dispersion of particles inside the gas.[5]
2) The Basset force was neglected.[12]
3) The virtual mass was not considered[12]; i.e., the particle spin velocity is insignificant compared with the axial velocity.
4) The vapor pressure of yttria partially stabilized zirconia (YSZ) is approximately 1 atm. The computational study carried out here is for atmospheric plasma. Also, the particle temperatures encountered in this analysis is well below the boiling point of YSZ. Therefore, the particle vaporization was neglected.
5) Radiative heat transfer between plasma and particles were neglected.[13]

2.1.4 Particle Dynamics Equation. The forces acting on the particle govern the particle motion and trajectory. A force balance equation on the particle, in the Lagrangian reference frame equated the particle inertia with the significant forces acting on the particles. The force equation below summarizes the total forces, consisting of drag force (F_D) and inertia force.

$$m_p = \frac{du_p}{dt} = F_D \quad \text{(Eq 4)}$$

that is,

$$\frac{du_p}{dt} = \frac{18\mu}{\rho_p D_p^2}\frac{C_p Re}{24}(u - u_p) \quad \text{(Eq 5)}$$

where

$$R_e = \frac{\rho D_p |u_p - u|}{\mu} \quad \text{(Eq 6)}$$

and

$$C_D = a_1 + \frac{a_2}{R_e} + \frac{a_3}{R_e^2} \quad \text{(Eq 7)}$$

where a_1, a_2, a_3 terms are constants applicable for different ranges of R_e as given by Morsi and Alexander.[14]

2.1.5 Particle Energy Equation. Particle heating or cooling is governed by the net flux of heat transferred between the particles and the surrounding plasma. The heat balance equation for the particle governs the particle heating and hence its temperature. The energy balance equation states that the heat transfer from the plasma to the particle provides the energy required for heating up the particle and the latent heat of melting.

$$hA_p(T_\infty - T_p) = m_p c_p \frac{dT_p}{dt} + m_p H_{sf}\frac{d\zeta}{dt} \quad \text{(Eq 8)}$$

where ζ is the liquid fraction.

The heat transfer coefficient, h, was evaluated using the Ranz and Marshall[15] correlation:

$$N_u = \frac{hD_p}{k} = 2.0 + 0.6Re_D^{1/2}\mathrm{Pr}^{1/3} \quad \text{(Eq 9)}$$

2.1.6 Stochastic Particle Trajectory. The turbulent dispersion of particles was calculated using a stochastic discrete particle approach. The instantaneous value of the gas velocity fluctuation was used to predict the dispersion of particles due to turbulence. The "Random Walk Model"[7] was used to determine the instantaneous gas velocity, $u' = \xi\sqrt{\overline{u^2}}$, where ξ was the instantaneous random number generated.

The turbulent dispersion of particles was predicted by integrating the trajectory equation of individual particles using the

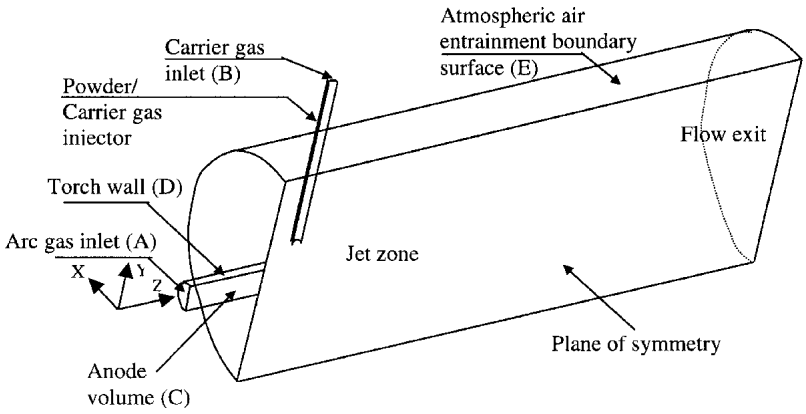

Fig. 1 Schematic diagram of plasma spray process with computational domain that consisted of anode, particle/carrier gas injector and the jet zone

Table 2 Boundary Conditions for Cases S1 to S6 in Table 3. A, B, C, D, and E can be Found in Fig. 1

Boundary, Fig. 1	S0	S1	S2	S3	S4	S5	S6
Arc gas flow rate at torch inlet (A), g/s	1.106	1.106	1.106	1.106	1.106	1.377	1.377
Carrier gas flow rate at carrier gas inlet (B), g/s	0	0.038	0.077	0.115	0.067	0.067	0.067
Heat source in energy equation at anode volume (C), $W/m^3/10^{10}$	3.237	3.237	3.237	3.237	3.237	3.237	2.543
Torch wall (D) velocity, m/s				0			
Plenum surface (E) temperature, K				300			
Plenum surface pressure, atm. (abs.)				1.0			
Turbulence intensity at torch inlet (A), %				5.05			
Turbulence intensity at carrier gas inlet (B), %				6.5			

instantaneous fluid velocity along the particle path during the integration.

2.2 Boundary Conditions

The boundary conditions for the plasma flow numerical model are given in Table 2. The conditions S1-S6 identify six cases for which the corresponding boundary conditions to the spray settings are depicted in Table 3. The torch wall was assumed to be adiabatic to avoid further heat loss from the nozzle because the total heat loss was accounted in the heat source term defined in the energy equation through torch efficiency.

2.3 Solution Procedures

The three-dimensional computational domain is shown in Fig. 1. As there was a plane of symmetry with respect to the y-z plane, only half the physical domain was modeled.

Fluent V5.4 code (Fluent Inc., Lebanon, NH) was used to solve the system of conservation equations using the control volume-finite element method. The grid generated for the computational domain included the plasma torch, powder/carrier gas injector, and the plasma jet region. The flow field was solved using the SIMPLE algorithm developed by Patankar.[16]

The computational domain consisted of the anode (D), the jet zone, and the powder/carrier gas port. The size of anode was $\phi 7.5 \times 18.5$ mm, the jet zone was $\phi 70 \times 220$ mm, and that of the carrier gas port was $\phi 2.2 \times 50$ mm. The injector port was located 7 mm from the nozzle exit and 9 mm above the nozzle axis. The governing equations were solved using a grid having sizes 14 x 24 x 27 for the nozzle, 70 x 24 x 120 for the free jet, and 8 x 18 x 63 for the powder/carrier gas injector. The cell size in the mesh ranged from 0.5 x 0.5 x 0.44 mm at the jet exit and 1.8 x 3.5 x 4.2 mm at the farthest corner of exit of the flow domain. These cell sizes were found to be optimum with respect to the minimum number of grids, after checking for spatial convergence with various grid sizes.

Based on the typical values of operation for the Metco 3 MB (Sulzer Metco Inc., Westbury, NY) torch,[17] the parameters listed in Table 3 were selected for the numerical study.

Table 3 Process Parameters for Numerical Computations Correspond to Boundary Conditions in Table 2

Cases	S0	S1	S2	S3	S4	S5	S6
Torch power input, kW	42	42	42	42	42	42	33
Primary gas (Ar) flow rate, slm	40	40	40	40	40	50	50
Secondary gas (H_2) flow rate, slm	12	12	12	12	12	11	11
Carrier gas flow rate, slm	0	2.0	4.0	6.0	3.5	3.5	3.5

Table 4 Physical and Thermal Properties of Yttria Stabilized Zirconia[18]

Property	ρ, kg/m3	T_{mp}, °C	T_{bp}, °C	ΔH_{sf}, J/kg	C_p, J/kgK	k, W/mK
Value	5890	2700	5000	710 000	*	2.4

*$C_p = 1.06343 \times 10^{-6}\ T_p^3 - 2.188953 \times 10^{-3}\ T_p^2\ 1.709671\ T_p\ 1.466367 \times 10^2\ 273 < T_p < 873\ C_p = 678.5\ T_p > 873$

In the first phase of solution, the plasma flow with carrier gas was simulated. The known velocities and temperatures of the gas were used for the second phase when the particles were introduced. The particles were introduced with zero velocity at the inlet of the carrier gas injector. The drag law as indicated in Eq 4-7 was applied and the particles were injected to the plasma jet with the injection velocity as computed by the equations of particle dynamics described in the section "Particle Dynamics Equation" above. Cases S1-S4 were performed to study the effect of carrier gas flow rate on the particle behavior. Cases S4 and S5 were performed to study the effect of arc gas flow rate and volume fraction of H_2 on particle behavior. Cases S5 and S6 were performed to study the effect of torch power input on the particle behavior. The simulation results reported in this work are at a standoff distance of 80 mm.

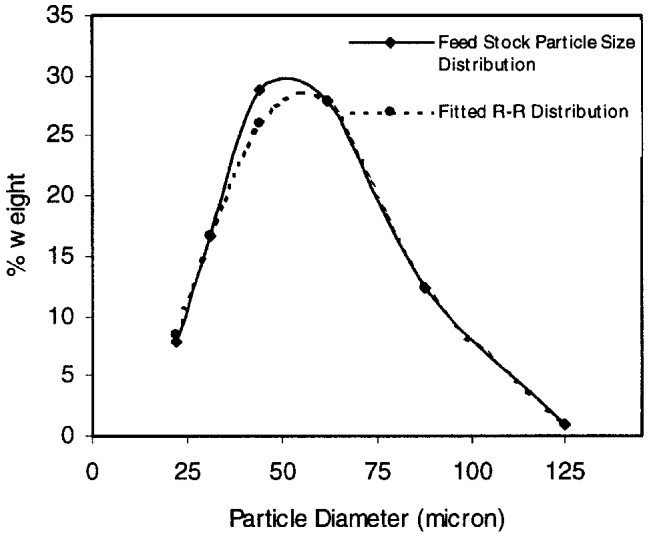

Fig. 2 The particle size distributions for the as received spray powder and the fitted R-R distribution

2.4 Property Variation

In plasma spraying, a large temperature variation occurs inside the cathode-anode region and in the plasma jet. Therefore, property variation with respect to the temperature has to be included. The transport properties for viscosity, specific heat, and thermal conductivity were entered as a function of temperature based on the data of Boulos et al.[8] These values had been incorporated in the program as linear piecewise profiles with respect to temperature and permitted the determination of these properties for the cell temperature obtained at every iteration.

The particles used in the simulation are the yttria stabilized zirconia (METCO 204 NS, Sulzer Metco Inc., Westbury, NY). The physical and thermal properties[18] are as shown in Table 4.

2.5 Particle Size Distribution

The mass distribution of particles was assumed to follow a Rosin-Rammler (R-R) distribution.[12] Here, the R-R distribution was fitted to the actual feedstock size distribution[17] with the aim of verifying the simulation with experimental spray trial[1] already conducted. An exponential relationship exists between the particle diameter, D, and the mass fraction M_D of particle diameters greater than D:

$$M_D = \exp\left[-\left(\frac{D}{\overline{D}}\right)^n\right] \quad \text{(Eq 10)}$$

where $\overline{D}$ and n refer to the mean diameter and spread factor, respectively. The spread factor and mean diameter for the calculations are 2.3489 and 65.3 μm, respectively. The fitted and actual size distribution for the current analysis is shown in Fig. 2.

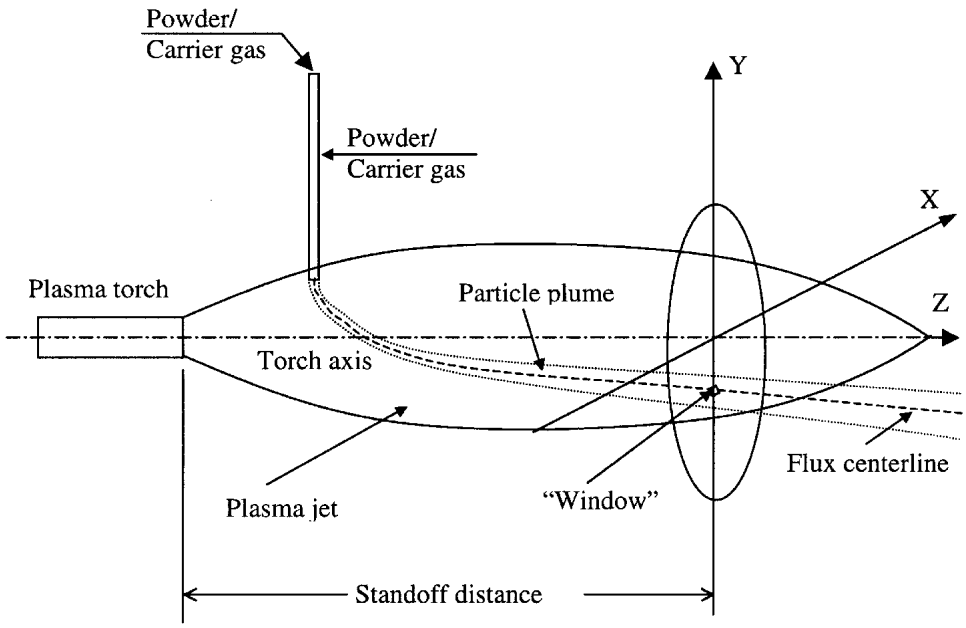

Fig. 3 Schematic diagram for the illustration of the "window" in the centerline measurements and simulation

2.6 Particle Plume Centerline Values

The "flux centerline" is defined as an imaginary line in the particle plume, where the particle number concentration is maximum. It can be obtained at any cross-sectional location by transversing through the particle plume where the particle number flux is at maximum. The position of the peak concentration is determined from the count of all particles passing through the "window" at the standoff distance of 80 mm. The locus of these points is the centerline of the peak concentration, which need not correspond to the centerline of the plasma spray torch. The "window" size had been fixed at 1 x 1 mm. Temperature, velocity, and size frequency distribution were plotted for the window of maximum particle flux. The co-ordinate for the window could be ascribed as (0, y_d, sd), where, 'y_d' is the y co-ordinate of maximum flux which changes as carrier gas flow rate is varied, and 'sd' is the standoff distance. Hereafter, centerline values refer to the mean values of particle parameters at the maximum flux widow with a standoff distance of 80 mm.

2.7 Data Analysis of FLUENT Output

It is necessary to process the data generated by FLUENT into a form suitable for comparison with experimental data. All the particles passing through the maximum flux window were counted irrespective of their size and statistically analyzed to find the mean of temperature, velocity, and size. The count of all the particles from 1500-4500 °C with set size interval of 25 °C was summarized. Particles with velocities ranging between 50 and 450 m/s at intervals of 5 m/s were counted to generate the velocity distributions. For particle diameter distributions, particles with size ranging between 20 and 125 μm at intervals of 2 μm was counted. From the distributions generated above, number averaged particle temperature, velocity and size were calculated using the following statistical equations.

$$Mean = \frac{\sum_{i=1}^{N} n_p \phi}{\sum_{i=1}^{N} n_p} \quad \text{(Eq 11)}$$

$$SD = \sqrt{\frac{\sum_{i=1}^{N} n_p \phi^2 - \frac{\left(\sum_{i=1}^{N} n_p \phi\right)^2}{\sum_{i=1}^{N} n_p}}{\sum_{i=1}^{N} n_p - 1}} \quad \text{(Eq 12)}$$

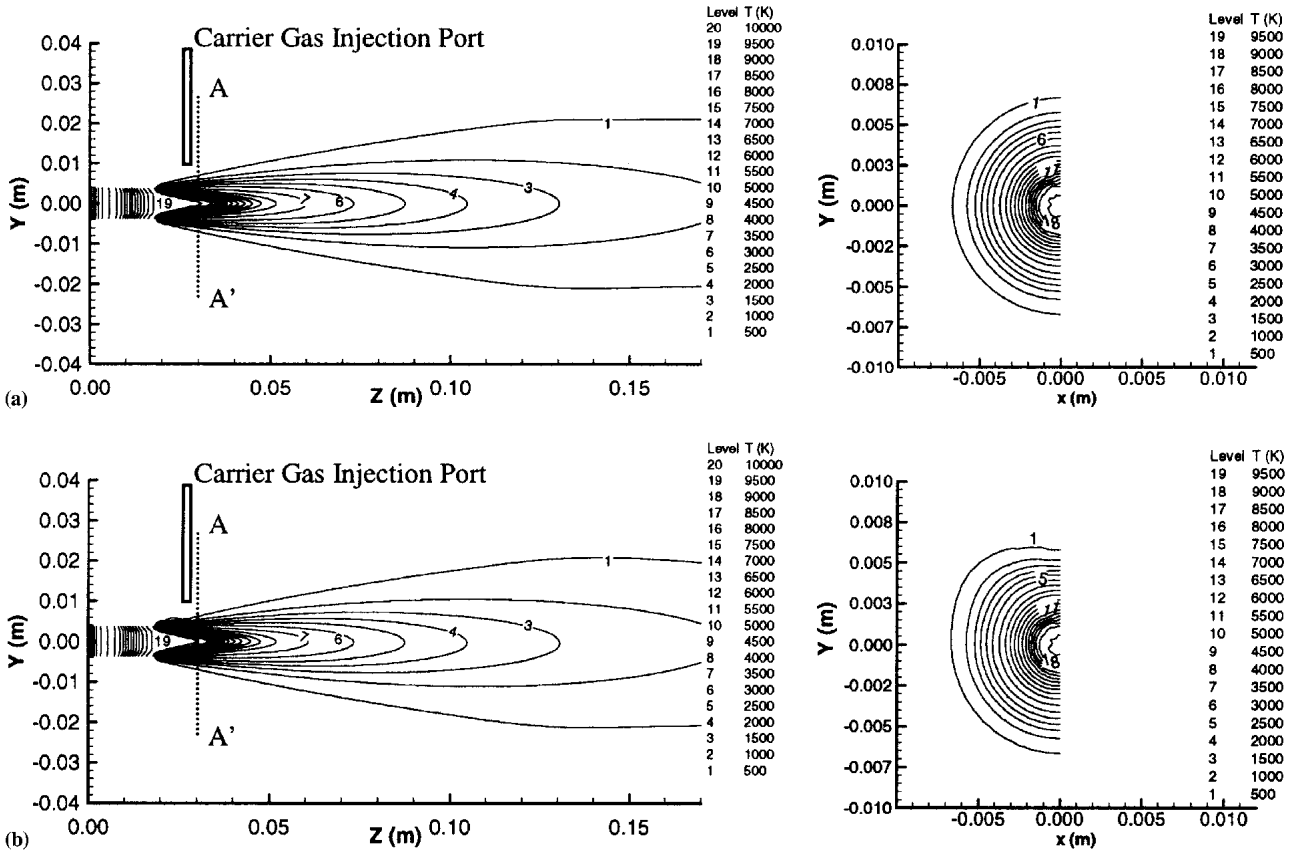

Fig. 4 **(a)** The isotherms of plasma plume at the plane of symmetry and at a cross section (A-A′), 3 mm away from the carrier gas port for case S0 (without carrier gas injection). **(b)** The isotherms of plasma plume at the plane of symmetry and at a cross section (A-A′), 3 mm away from the carrier gas port for case S3 (with carrier gas injection of 6 slm).

where, *Mean* is the number average of particle in-flight parameters, viz. temperature, velocity and size, ϕ is the interval mean, n_p is the interval count, N is the total number of interval counts, and *SD* is the standard deviation.

The computational results are deterministic in nature. The particles are simulated essentially as single particles. Although multi-particle injection is used, it is essentially single particle simulation due to the assumption of zero particle-to-particle interactions. However, the advantage is that the entire size distribution in the feedstock can be injected simultaneously as a realistic distribution and individual particles within a selected size range can be tracked in terms of all physical parameters such as temperature, velocity, size, and trajectory.

The size distribution in a realistic feedstock can be divided into a number of sub divisions; each sub division delimits a specific size range. The larger number of sub-divisions implies a smaller range in particle sizes for each division and a higher resolution of the numerical analysis. The particle feedstock between 22-125 μm and a size interval of 1 μm was injected from the surface of the carrier gas inlet port (Fig. 1).

The deterministic process has the ability to track all particles such that at any location in the plasma plume, the number of particles and their size that pass through the "window" (Fig. 3) can be determined. Therefore, a similar statistical distribution to the experimental measurements would be produced. FLUENT also has a stochastic model that allows a particle to be perturbed so that it travels along a slightly different trajectory from another particle similar in size and injection velocity. The two particles will, therefore, not strike the substrate at exactly the same spot but at two points that are slightly apart.

3. Results and Discussion

The effects of carrier gas on the plasma jet as well as on the particles are analyzed in the following sections. The effects of other process parameters on particle behavior will be discussed in later sections.

3.1 Effects of Carrier Gas on the Plasma Jet Behavior

The predicted temperature and velocity distributions for cases S0 and S3 at the plane of symmetry are shown in Fig. 4 and 5 respectively. In case S0, there was no carrier gas injection whereas the carrier gas flow rate was at 6 slm for case S3. These two cases served as reference cases to study the effects of carrier gas flow rate on the plasma jet.

The carrier gas affects the plasma plume by cooling down and retarding the plasma jet at the immediate vicinity of the carrier gas injector exit. Comparing the jet cross sections in Fig. 4(b) and 5(b), the jet symmetry with respect to the x-z plane is

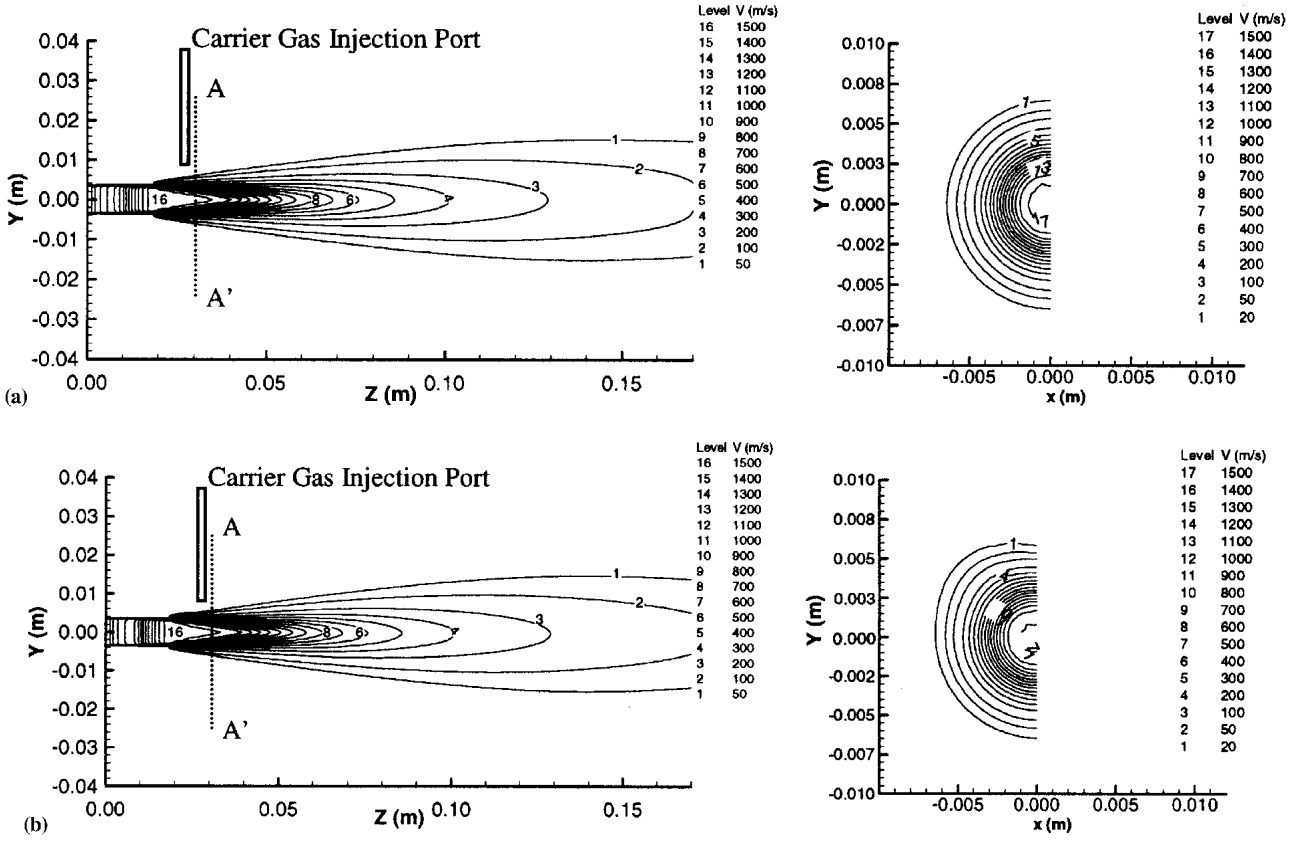

Fig. 5 **(a)** The axial velocity contour of plasma plume at the plane of symmetry and at a cross section (A-A″), 3 mm away from the carrier gas port for case SO (without carrier gas injection). **(b)** The axial velocity contour of plasma plume at the plane of symmetry and at a cross section (A-A″), 3 mm away from the carrier gas port for case S3 (with carrier gas injection of 6 slm)

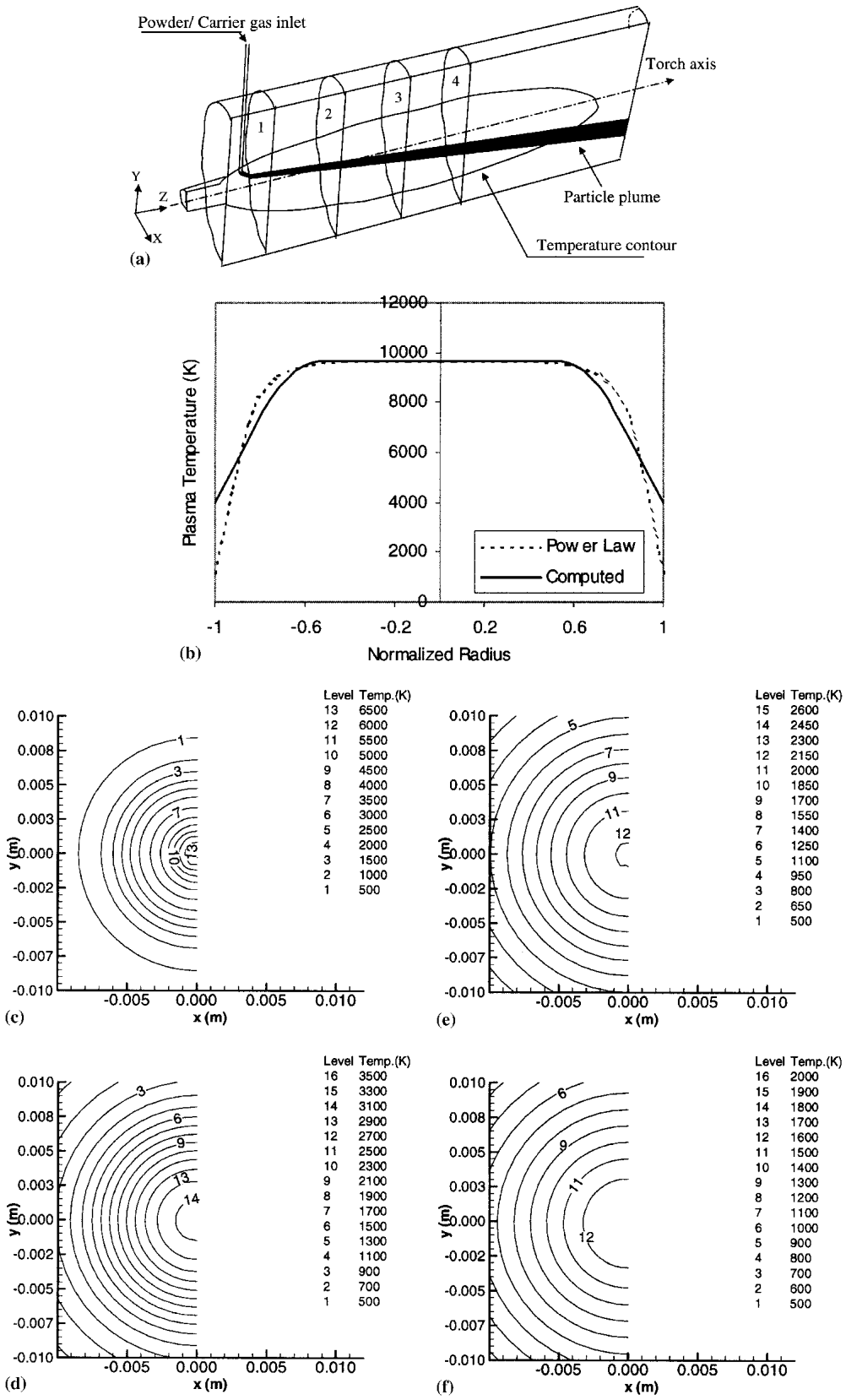

Fig. 6 **(a)** Schematic of the particle injection process. **(b)** Temperature profiles fitted by power law and the computed temperature profiles at 2 mm away from the nozzle exit in axial direction. **(c)** Section 1, temperature at 20 mm away from nozzle exit. **(d)** Section 2, temperature at 50 mm away from nozzle exit. **(e)** Section 3, temperature at 80 mm away from nozzle exit. **(f)** Section 4, temperature at 100 mm away from nozzle exit

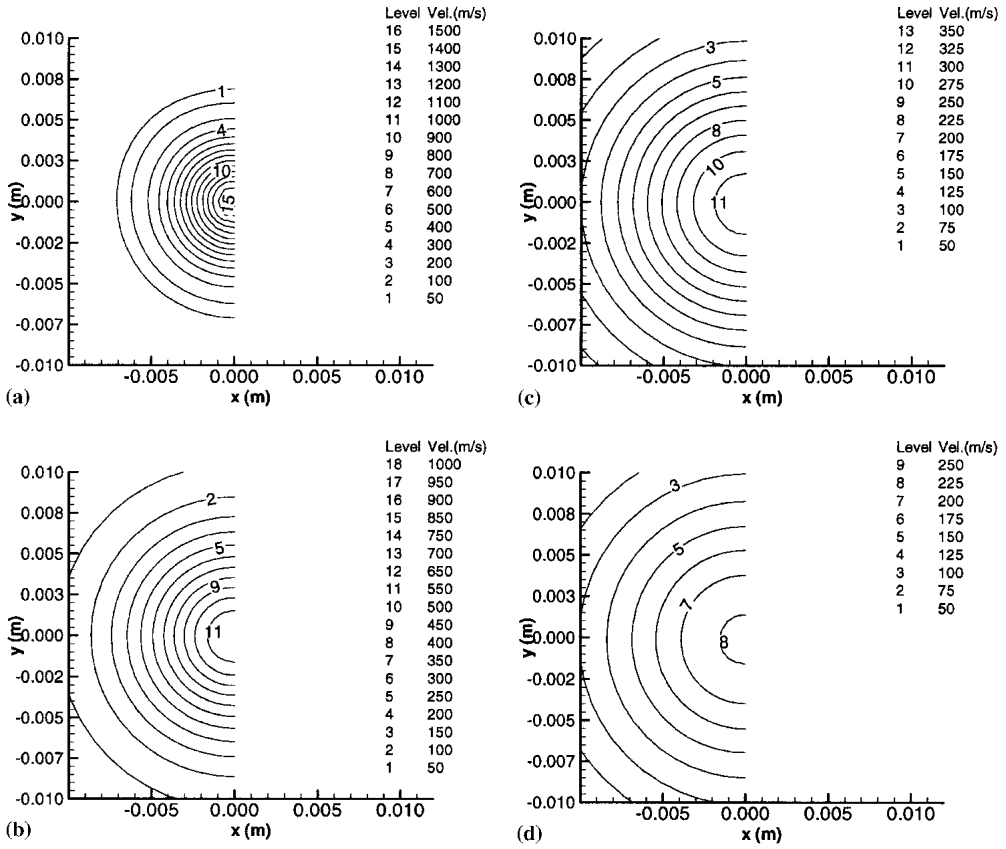

Fig. 7 Velocity contours at various cross section of the plasma plume. **(a)** Section 1, velocity at 20 mm away from nozzle exit. **(b)** Section 2, velocity at 50 mm away from nozzle exit. **(c)** Section 3, velocity 80 mm away from nozzle exit. **(d)** Section 4, velocity at 100 mm away from nozzle exit

affected by the injection of carrier gas that causes the contours to be displaced downwards. It is, however, noted that the jet core is almost unaffected by the injection of carrier gas. This can be understood by the fact that the momentum of the plasma jet is much higher than that of the carrier gas that prevented penetration of the carrier gas into the jet core.

3.2 Velocity and Temperature Contour at Various Plasma Plume Cross Sections

The temperature profile at 2 mm away from the nozzle exit for the case S4 is shown in Fig. 6(b). It was found that the value 8 for the index (m) could be fitted for this case with centerline value (T_0) as 9645 K in the power law

$$T = (T_0 - T_w)\left[1 - \left(\frac{x}{R_i}\right)^m\right] + T_w$$

This shows that the temperature profiles generated in the present model with the assumption of arc gas heating through the source term in energy equation are in reasonable agreement with those generated by power law.

Figure 6(c-f) and 7 present the isotherms and velocity contours for case S4 at various sections from the nozzle exit. At this carrier gas flow rate of 3.5 slm, it is observed that the symmetry of the plasma jet is unaffected by the carrier gas flow rate, except

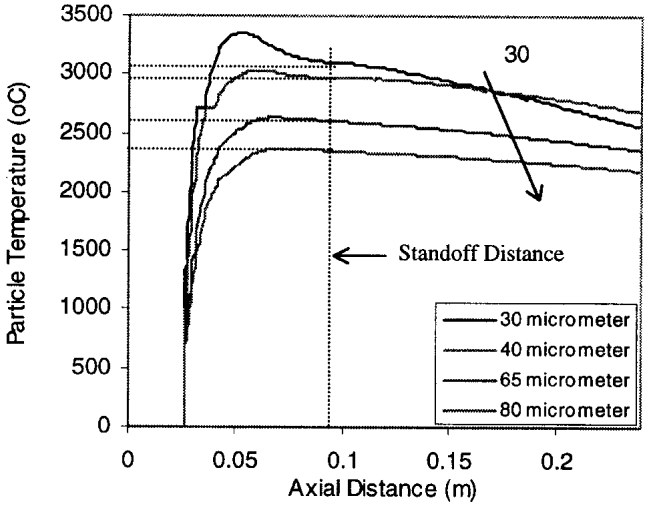

Fig. 8 In-flight particle temperature along the axial distance for case S4

near the section at the immediate vicinity of the carrier gas injector. Based on the results shown in Fig. 4-7, it could be concluded that plasma cooling by the carrier gas jet is minimal in the case of the external injection mode except at the edge of the planar jet. However, it should be pointed out that this might not

Table 5 Comparison of Simulation Centerline Temperature With Experimentally Measured Values by Kucuk et al.[1]

Case	Measured Centerline Temperature, °C	Maximum Temperature, °C (*A*)	Simulated Centerline Temperature, °C	Maximum Temperature, °C (*B*)	% Variation $B - A/A \cdot 100$
S1	2432 ± 325	2757	2906 ± 240	3146	14.1
S2	2538 ± 373	2911	3201 ± 221	3422	17.6
S3	2524 ± 371	2895	3217 ± 310	3527	21.8
S4	2577 ± 446	3023	3054 ± 275	3329	10.1

be the same for internal injection in which the carrier gas injection is very close to the nozzle axis.

3.3 Particle Behavior

In the following sections, the particle temperature, velocity, and size at the centerline will be analyzed. Initially, comparison of the computational results with those of the experimental measurement[1] will be presented. Based on the accuracy of results, a detailed analysis of the particle behavior and their dependence on process parameters will be discussed.

3.4 Comparison of Simulation Values With Experimental Measurements at the Centerline

The experimental results reported by Kucuk et al.[1] will first be compared in this section to verify the accuracy of the computed results. The measurements were carried out on the in-flight diagnostic system DPV-2000 (Tecnar Automation, St. Hubert, QC, Canada). This system is capable of measuring the velocity, temperature and size of the particles in-flight at any location within the particle plume. A large number of particles were "sampled" to obtain mean temperature, velocity, and size data. This implies that the particle "temperature" "velocity," and "size" are not of one particular single sized particle, but rather it is a statistical distribution in which the parameter observed is sampled over many particles that pass through the measurement volume shown in Fig. 3. The particle count includes particles of various sizes of the feedstock (typically between 22-125 μm). The mean velocity and temperature are obtained by taking the mean of the distribution.

The simulation and measurement in general agrees closely for all cases considered with case S4 showing the best agreement. As such, case S4 will be used for further comparison.

3.5 Comparison of Measurement and Simulation Techniques at the Centerline

As mentioned earlier, comparison of simulation and experimental results must be assessed from a different perspective. In the numerical simulation, the centerline "window" counts every particle passing through it to calculate the number averaged particle temperature. On the other hand, experimental measurements using the DPV-2000 considers only the particles that pass through the two-slit mask, whose trajectory is completely included within the control volume (slit area × depth of field) of the measured field. The system does not take into account particles above the upper limit of the particle analysis rate of the system, which are 400 particles per second.[19] Thus, a relatively smaller number of particles were counted during the physical measurement, whereas in simulation all the particles that pass through the "window" will be counted and included in the calculation of mean values.

For the comparison of simulation and experimental values of temperature, consider Fig. 8 where the simulated temperature of individual sized particles on reaching the substrate at a standoff distance of 80 mm is shown. In case S4, the experimental centerline particle temperature is 2577 ± 446 °C and that of simulation is 3054 ± 275 °C (Table 5). The temperature for 30, 40, 65, and 80 μm particles is 3093, 2968, 2596, and 2347 °C, respectively.

For the comparison of particle velocity, consider Fig. 9 where the velocity of individual sized particles as a function of axial distance is given. The experimental centerline particle velocity at a standoff distance of 80 mm is 165 ± 73 m/s and that of simulation is 230 ± 47 m/s (Table 6). The velocity of particles of 30, 40, 65, and 80 μm particles is 275, 224, 154, and 131m/s, respectively.

Based on the comparison on the particle temperature and velocity, it can be seen that the temperature and velocity of individual sized particles can vary widely compared with the mean values of velocity and temperature at the centerline. The simulated values essentially encompassed the range attained in the experiment. It should be pointed out that, in the actual plasma spraying process, the radial component of particle injection velocity may not be negligible. The particles exiting from the injector exhibit a large dispersion angle (up to a 30° cone angle) resulting from their collision with the injector wall as reported by Vardelle et al.[10] This dispersion may play an important role in the trajectory distribution. Also, in the actual spraying process, there may exist inter-particle interactions, which may result in coalescence of molten particles, break up or blending of the particles of different sizes. But, these effects were not included in the simulation. Therefore, the above two issues can lead to an increased dispersion of the particle plume. This would result in the presence of particles of all sizes in the measurement volume and that may affect the simulated mean values of particle temperature, velocity and size.

3.6 Simulated Particle Temperature at the Centerline

Figure 10 illustrates the variation of particle centerline temperature for cases S1-S6 at a standoff distance of 80 mm. It is evident that particle temperature first increases with increase in carrier gas flow rate, but decreases as the latter is increased further. When the carrier gas flow rate increased from 2 slm (S1) to 4 slm (S2), the particle temperature increased from 2906-3217 °C (about 10%). The particle temperature is found to be at

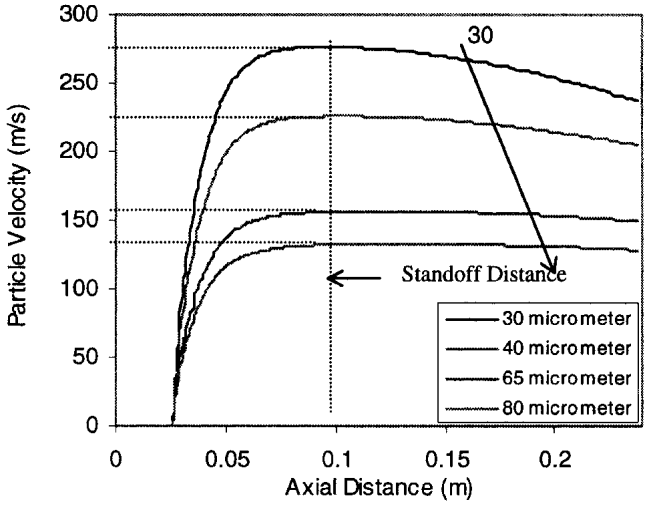

Fig. 9 In-flight velocity temperature along the axial distance for case S4

Table 6 Comparison of Simulation Centerline Velocity With Experimentally Measured Values by Kucuk et al.[1] for Case S4

Case	Measured Centerline Velocity, m/s	Maximum Centerline Velocity, m/s (*A*)	Simulated Centerline Velocity, m/s	Maximum Centerline Velocity, m/s (*B*)	% Variation $B - A/A \cdot 100$
S4	165 ± 73	238	230 ± 47	287	20.6

maximum for cases S2 among the first four cases, which clearly indicates that the particle trajectory was confined within the plasma core for the carrier gas flow rate at 4.0 slm.

From the particle temperature distribution shown in Fig. 10, it can be deduced further that the particle count with higher temperature increases progressively as the carrier gas flow rates were set to 2 slm, 3.5 slm, 4 slm, and 6 slm for cases S1, S4, S2, and S3, respectively. This phenomenon has to be interpreted in conjunction with the centerline particle size distribution as shown in Fig. 11. It can be seen that the particle count with smaller sizes increase with an increase in carrier gas flow rate. The implication is that an increase in carrier gas flow rate resulted in a better particle dispersion[20] and hence populating the centerline with smaller sized particles. This causes an increase of the centerline particle temperature since smaller sized particles attain higher temperature.

Another observation is that for case S5, there is a relatively narrow distribution of temperature (Fig. 10) and particle size (Fig. 11). The standard deviation of temperature is at minimum in case S5. An increase in total arc gas flow rate has prevented the dispersion of the particle plume in the lateral (i.e., *x*-axis) direction. This occurs because the higher momentum of the plasma plume subdued the radial component of the particle velocity and hence the particle dispersion.

Comparing case S5 with S6 (Fig. 11), there is an increase in particle dispersion with respect to the decrease in torch power. Reduction in torch power input resulted in the decrease in arc gas velocity and hence the particles were swept less readily in the axial direction in case S6 as compared with case S5.

3.7 Simulated Particle Velocity at the Centerline

Figure 12 illustrates the variation of particle centerline velocity for cases S1-S6. It can be seen that the particle velocity first increases from 220-256 m/s (about 16.5%) with an increase in carrier gas flow rate from 2-4 slm. The velocity decreases to about 202 m/s (by 20% compared with case S2) as it is increased further to 6 slm.

The particle velocity is found to be at maximum for cases S2 and S4. This indicates that the particle trajectory is confined within the plasma core for a carrier gas flow rate between 3.5 and 4.0 slm. For the low carrier gas flow rate case S1, the particles did not penetrate into the plasma core and hence attained a lower velocity and temperature. For higher carrier gas flow rate case S3, the particle plume crossed over the plasma core and resulted in the lower residence time within the high temperature plasma jet core.

3.8 Simulated Particle Size Distribution at the Centerline

Mean particle diameter at the centerline showed a decreasing trend in mean particle size with increase of carrier gas flow rate until 4slm, for cases S1, S4, and S2. Also, the particle count passing through the centerline window exhibited an increasing trend as the carrier gas flow rate increased. But the trend was reversed as the carrier gas flow rate was further increased to 6 slm in case S3. This is due to the increased particle dispersion at higher carrier gas flow and, hence, the possibility of capturing particles with higher sizes which are low in count.

Comparing cases S4 and S5, it can be seen in Fig. 11 that the mean particle size decreased as the total arc gas flow rate was increased from 52-61 slm. This can be explained in such a way that the increased arc gas flow in case S5 prevented particle dispersion which resulted in a narrower particle plume and, hence, the capture of more particles at the centerline window.

Comparing cases S5 and S6, it can be seen that the particle count was decreased and mean size increased as the torch power decreased from 42-33 kW. This is due to the fact that the decreased torch power resulted in lower plasma plume velocity and an increased particle dispersion.

3.9 Effects of Other Process Parameters on Particle Behavior

Other than the carrier gas flow rate, process parameters such as power input, arc gas flow rate, and volume fraction of H_2 will also affect the particle behavior. Comparing cases S5 and S6 (Fig. 10 and 12) it can be seen that both particle velocity and temperature decreased as power input decreased. Particle temperature decreased from 2685-2615 °C (3%) and velocity decreased from 249-229 m/s (8%). The decrease in power input results in a decrease of energy density of the arc gas for the same arc gas flow rate. It is found that with all the other parameters remaining the same, an increase in arc gas flow rate would result in an increase in particle velocity accompanied by a decrease in particle temperature.

Comparing cases S4 and S5 (Fig. 12), it can be seen that average particle velocity at the centerline increased (230 ± 47 m/s for case S4 and 249 ± 47 m/s for case S5). For the same cases, the particle temperature decreased from 3054 ± 275-2877 ±

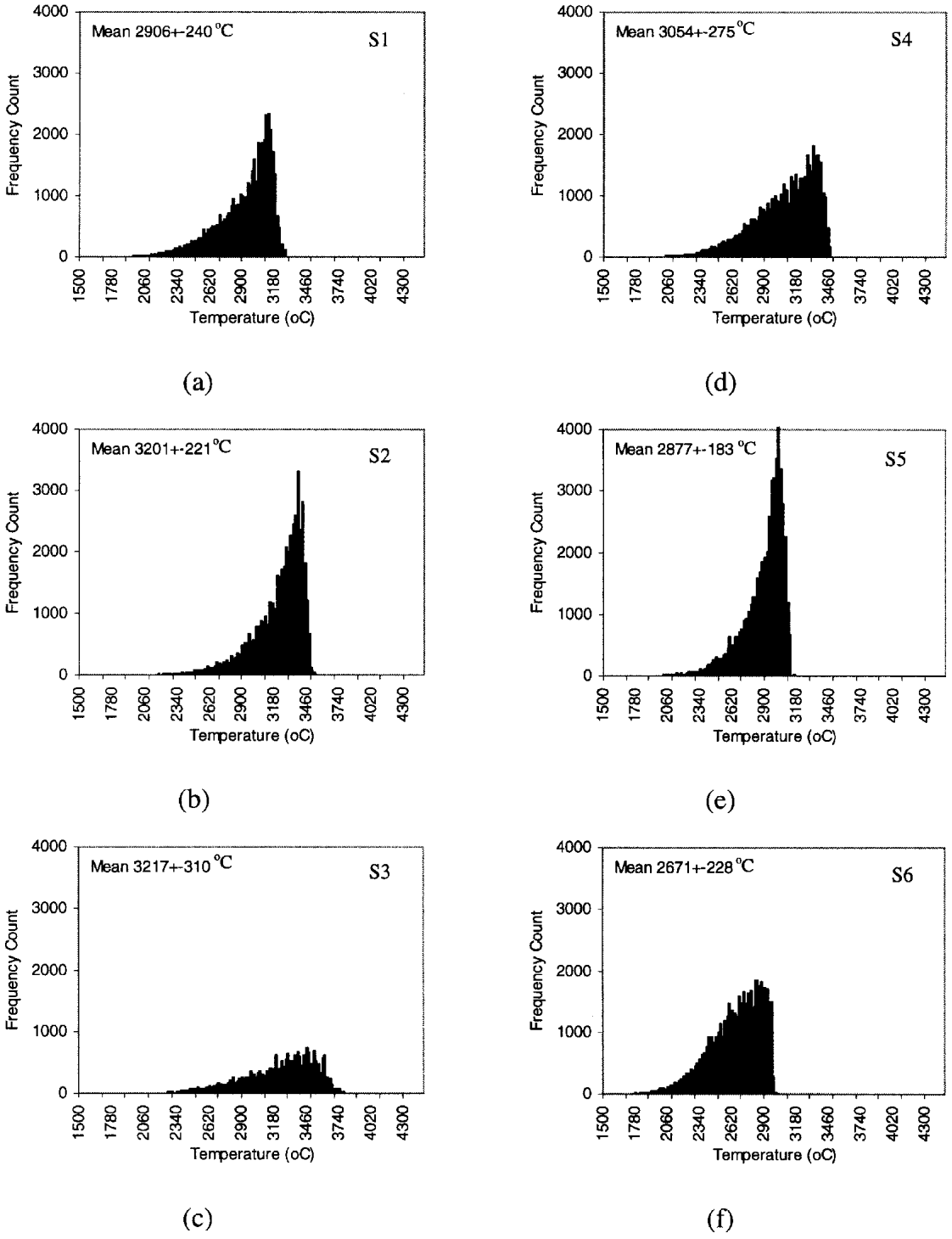

Fig. 10 Simulated centerline temperature distribution for cases S1-S6

183 °C (a 12.1% reduction) as shown in Fig. 10. It should be pointed out that the same trend is observed in the experiments in which the particle temperature decreased significantly from 2577 ± 446 °C for case S4-2326 ± 310 °C for case S5 (a 9.7% reduction). The decrease in particle temperature arises due to the decrease in energy density of the arc gas at the same power level.

4. Conclusions

A numerical investigation on particle behavior with variation of power input, carrier gas flow rate, arc gas flow rate, and mol fraction of H_2 in an Ar-H_2 plasma spray system have been performed. The numerical results were compared with ex-

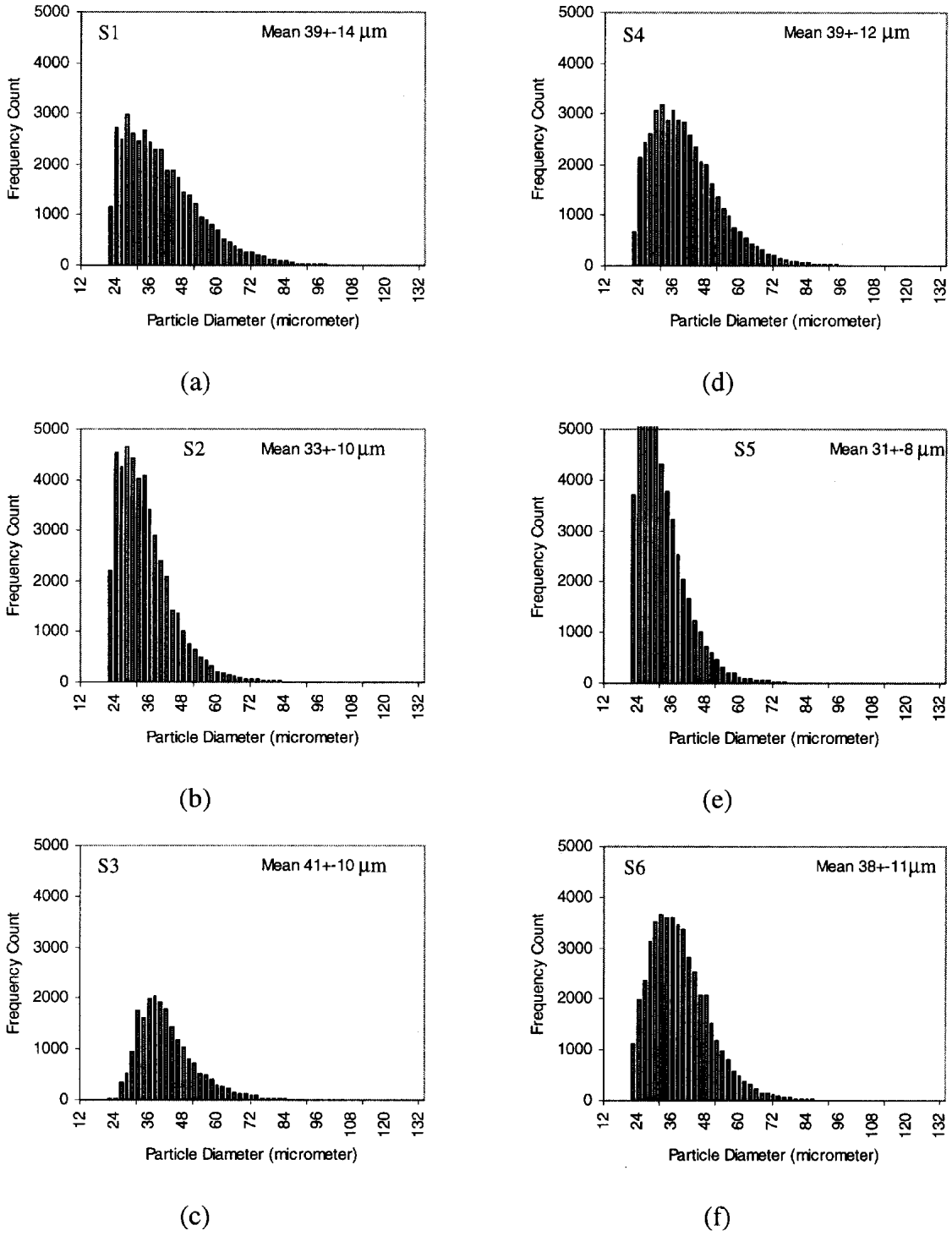

Fig. 11 Particle size distribution at centerline for cases S1-S6

perimental in-flight particle parameter measurements of Kucuk et al.[1] Reasonably good agreement between the numerical predicted values and the experimental measurement has been obtained for certain cases while other cases demonstrated similarity in the general trends. Particle temperature and velocity were shown to be strongly dependent on carrier gas flow rate.

It was found that the quenching of arc gas by carrier gas was not significant for the cases considered, especially in the plasma core. It can be concluded that the in-flight particle behavior varied only with variation of injection velocity and hence the momentum acquired by particles from the carrier gas flow rate.

The particle temperature, velocity, and size inside the plasma

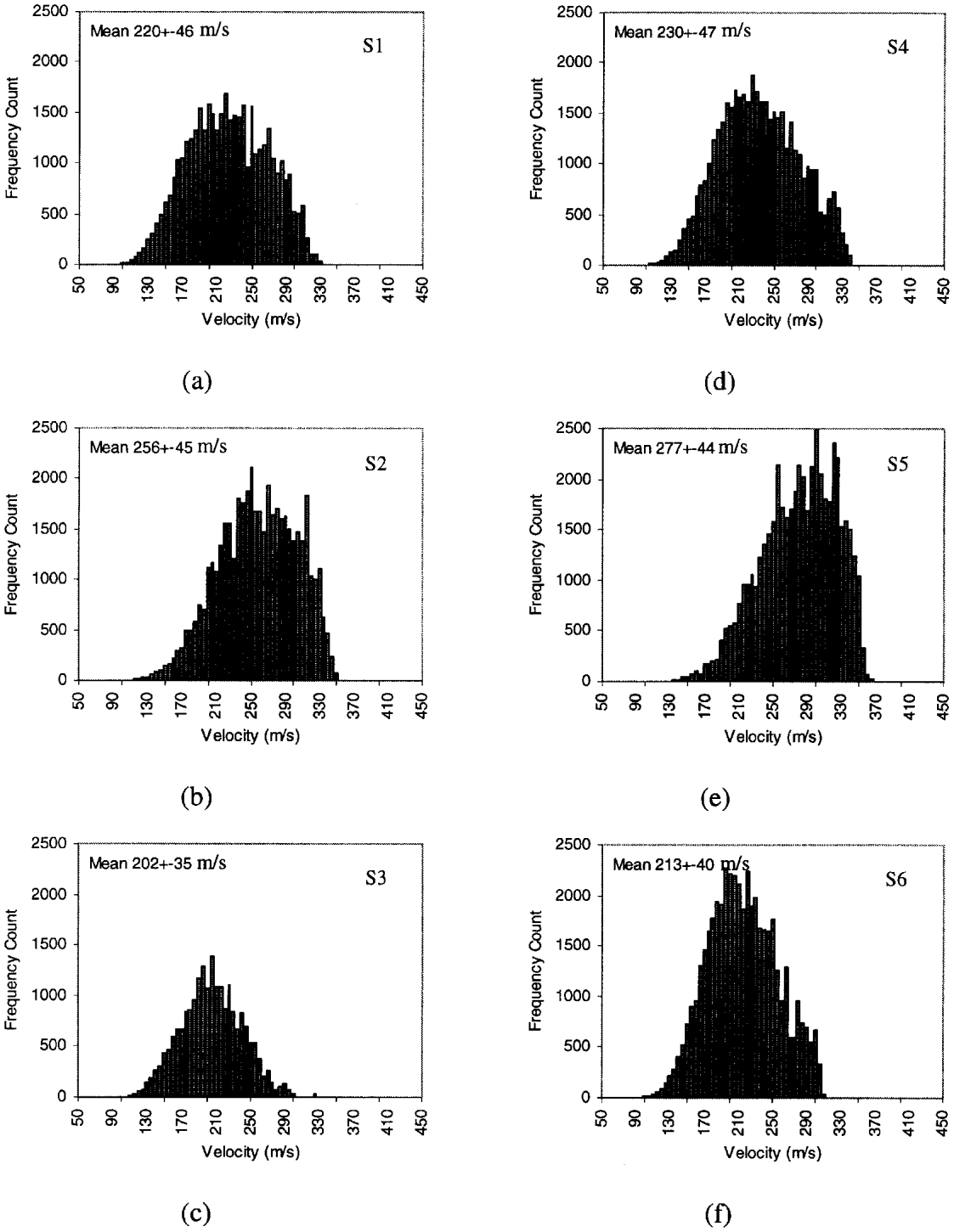

Fig. 12 Simulated velocity distribution at centerline for cases S1-S6

plume at a specified standoff distance at 80 mm have been investigated. The results showed that carrier gas flow rate variation from 2-4.0 slm can increase the centerline particle mean temperature and mean velocity to a maximum of 10% and 16%, respectively, at the specified standoff distance. A further increase of carrier gas flow rate to 6 slm did not cause any change to the particle temperature, but the particle velocity would be decreased by 20%. It was also found that an increase in the total arc gas flow rate from 52-61 slm, with all other process parameters remained unchanged, resulted in higher particle velocity by 17%, but lower particle temperature by 6%. For a given process parameter setting, the kinetic and thermal energy extracted by the particles was at their maximum for carrier gas flow rate at about 3.5-4.0 slm.

A contribution of this study is the development of a comprehensive model to predict the three-dimensional behavior of plasma spray with carrier gas interaction with plasma plume and the simultaneous injection of multi-sized particle. The methodology adopted in presenting the results is unique. Simulation results can be used to directly compare with the experimental results. With the concept of "window," particle parameters were statistically analyzed, instead of the presentation as that of single sized particle.

Acknowledgment

The first author (KR) takes this opportunity to thank Nanyang Technological University, Singapore, for financial support to perform this research through fund AcRF: 26/96.

References

1. A. Kucuk, R.S. Lima, and C.C. Berndt: Influence of Plasma Spray Parameters on In-Flight Characteristics of ZrO2-8 wt.% Y2O3 Ceramic Particles," *J. Am. Ceram. Soc.,* 2001, *84*(4), pp. 685-92.
2. Y.P. Wan, V. Prasad, G.-X. Wang, S. Sampath, and J.R. Fincke: "Model and Powder Particle Heating, Melting, Resoldification, and Evaporation in Plasma Spraying Processe*," J. Heat Trans.,* 1999, *121,* pp. 691-99.
3. I. Ahmed and T.L. Bergman: "Simulation of Thermal Plasma Spraying of Partially Molten Ceramics: Effects of Carrier Gas on Particle Deposition and Phase Change Phenomena," *J. Heat Trans.,* 2001, *123*(1), pp. 188-96.
4. C.B. Ang, H.W. Ng, S.C.M. Yu, and Y.C. Lam: "A Process Control Methodology for DC Plasma Spraying," *Plasma Chem. Plasma Process.*," 2000, *20*(3), pp. 325-42.
5. C.B. Ang, A. Devasenapathi, H.W. Ng, S.C.M. Yu, and Y.C. Lam: "A Proposed Process Control Chart for DC Plasma Spraying Process—Part II: Experimental Verification for Spraying Alumina," *Plasma Chem. Plasma Process.,* 2001, *21*(3), pp. 401-19.
6. R.L. Williamson, J.R. Fincke, and C.H. Chang: "A Computational Examination of the Sources of Statistical Variances in Particle Parameters During Thermal Plasma Spraying," *Plasma Chem. Plasma Process.,* 2000, *20*(3), pp. 299-324.
7. *The Fluent User's Guide*, 2000, Chapter 8, Fluent Inc., Lebanon, NH 03766.
8. M.I. Boulos, P. Fauchais, and E. Pfender: *Thermal Plasmas: Fundamentals and Application*, Vol. 1, Plenum Press: New York, NY, 1994.
9. J.F. Bisson, B. Gauthier, and C. Moreau: "Effect of Plasma Fluctuations on In-Flight Particle Parameters" in *Thermal Spray 2001: New Surfaces for a New Millennium, Singapore*, ASM International, Materials Park, OH, 2001.
10. M. Vardelle, A. Vardelle, and P. Fauchais: "Spray Parameters and Particle Behavior Relationships During Plasma Spraying," *J. Therm. Spray Technol*., 1993, *2(*1), pp. 79-91.
11. C.H. Chang and J.D. Ramshaw: "Numerical Simulations of Argon Plasma Jet Flowing Into Cold Air," *Plasma Chem. Plasma Process.,* 1993, *13*(2), pp. 189-209.
12. L.-S. Fan and C. Zhu: *Principles of Gas-Solid Flows*, Cambridge, UK, Cambridge University Press, 1998.
13. E. Bourdin and P. Fauchais: "Transient Heat Conduction Under Plasma Conditions," *Int. J. Heat Mass Trans.,* 1983, *26*(4), pp. 567-82.
14. S.A. Morsi and A.J. Alexander: "An Investigation of Particle Trajectories in Two-Phase Flow Systems," *J. Fluid Mech.,* 1972, *55*(2), pp. 193-208.
15. W.E. Ranz and W.R. Marshall: "Evaporation From Drops," *Chem. Eng. Prog.,* 1952, *48*(3), pp. 141-73.
16. S.V. Patankar: *Numerical Heat Transfer*, Hemisphere Publishing Corporation, Washington, DC, 1980.
17. Anon: *Tech-Report Metco 204NS Yttria Stabilized Zirconia Powder*, Metco, Westbury, NY, 1985.
18. J.F. Shackelford and W. Alexander, ed.: *The CRC Material Science and Engineering Hand Book*, CRC Press, Boca Raton, 1994.
19. L. Pouliot, P.J. Blain, and F. Nadeau: *DPV-2000 Reference Manual*, Tecnar Automation, St. Hubert, Canada, 1999.
20. K. Remesh, H.W. Ng, and S.C.M. Yu: "Influence of Process Parameters on the Deposition Footprint in Plasma Spray Coating," *J. Therm Spray Tech.,* 2003, *12*(3), pp. 377–392.